In Vivo Compatibility of Graphene Oxide with Differing Oxidation States

Stefanie A. Sydlik,[†,¶] Siddharth Jhunjhunwala,[†,∥,¶] Matthew J. Webber,[†,∥,¶] Daniel G. Anderson,[†,‡,§,⊥,∥] and Robert Langer*[,†,‡,§,⊥,∥]

[†]Koch Institute for Integrative Cancer Research, [‡]Department of Chemical Engineering, [§]Institute for Medical Engineering and Science, and [⊥]Harvard-MIT Division of Health Sciences and Technology, Massachusetts Institute of Technology, Cambridge, Massachusetts 02139, United States and [∥]Department of Anesthesiology, Boston Children's Hospital, Harvard Medical School, Boston, Massachusetts 02115, United States. [¶]S.A.S., S.J., and M.J.W. contributed equally.

ABSTRACT Graphene oxide (GO) is suggested to have great potential as a component of biomedical devices. Although this nanomaterial has been demonstrated to be cytocompatible *in vitro*, its compatibility *in vivo* in tissue sites relevant for biomedical device application is yet to be fully understood. Here, we evaluate the compatibility of GO with two different oxidation levels following implantation in subcutaneous and intraperitoneal tissue sites, which are of broad relevance for application to medical devices. We demonstrate GO to be moderately compatible *in vivo* in both tissue sites, with the inflammatory reaction in response to implantation consistent with a typical foreign body reaction. A reduction in the degree of GO oxidation results in faster immune cell infiltration, uptake, and clearance following both subcutaneous and peritoneal implantation. Future work toward surface modification or coating strategies could be useful to reduce the inflammatory response and improve compatibility of GO as a component of medical devices.

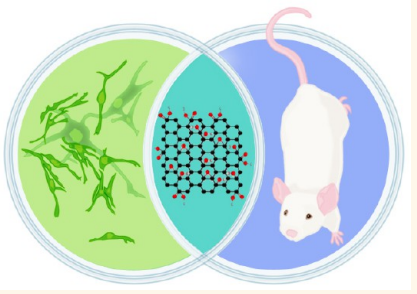

KEYWORDS: graphene oxide · graphene · biocompatibility · toxicity · *in vivo* · subcutaneous · intraperitoneal · immune response

Potential applications for graphene have been a source of great excitement in the field of nanotechnology, as its exceptional mechanical, electronic, and thermal properties[1] could contribute function as a component in polymer composites,[2] electronic devices,[3] or biomedical devices.[4] A preponderance of research on graphenic materials has focused on its oxidized state, graphene oxide (GO),[5] which is characterized by a high density of carboxylic acid, alcohol, and epoxide functional groups.[6] Though oxidation compromises the electronic[7] and mechanical[8] properties to an extent, it affords water dispersibility and chemical handles for covalent modification.[9,10] It is also generally thought that oxidation should improve compatibility for biological applications, due to the layer of water associated with the hydrophilic functional groups.[6,11] As such, GO has generated specific interest for use in preparing composite biomaterials,[12] photothermal therapies,[13−15] imaging modalities,[16] drug delivery strategies,[17,18] and cell-based tissue engineering substrates.[19,20]

The safety and compatibility of GO in tissue sites relevant for use in medical devices remain to be understood. Carbon nanotubes (CNTs), the cylindrical nanocarbon isotope of graphene, have been more thoroughly studied than graphene or GO in this regard. However, in spite of numerous efforts, no consensus has been reached regarding the safety of CNTs, with some studies finding these materials to be genotoxic or carcinogenic[21] and others finding them to be safe.[22] It is anticipated that the meta-stability and water dispersibility of GO may offer better prospects for biological compatibility than CNTs. GO is reported to be an autodegrading material on the time scale of months, with an aqueous degradation pathway resulting in the formation of humic acid.[23] This benign end product is the product of degradation of all organic matter and may be more easily cleared from the body.

Several studies have evaluated the toxicity of GO *in vitro*,[20,24−28] with a typical conclusion that the material is not cytotoxic. It has also been shown that GO may elicit a Toll-like receptor-mediated inflammatory response *in vitro*.[29,30] Assaying toxicity *in vitro* does not recapitulate the complexities of the physiologic milieu and attendant immune

* Address correspondence to rlanger@mit.edu.

Received for review December 10, 2014 and accepted April 7, 2015.

Published online April 07, 2015
10.1021/acsnano.5b01290

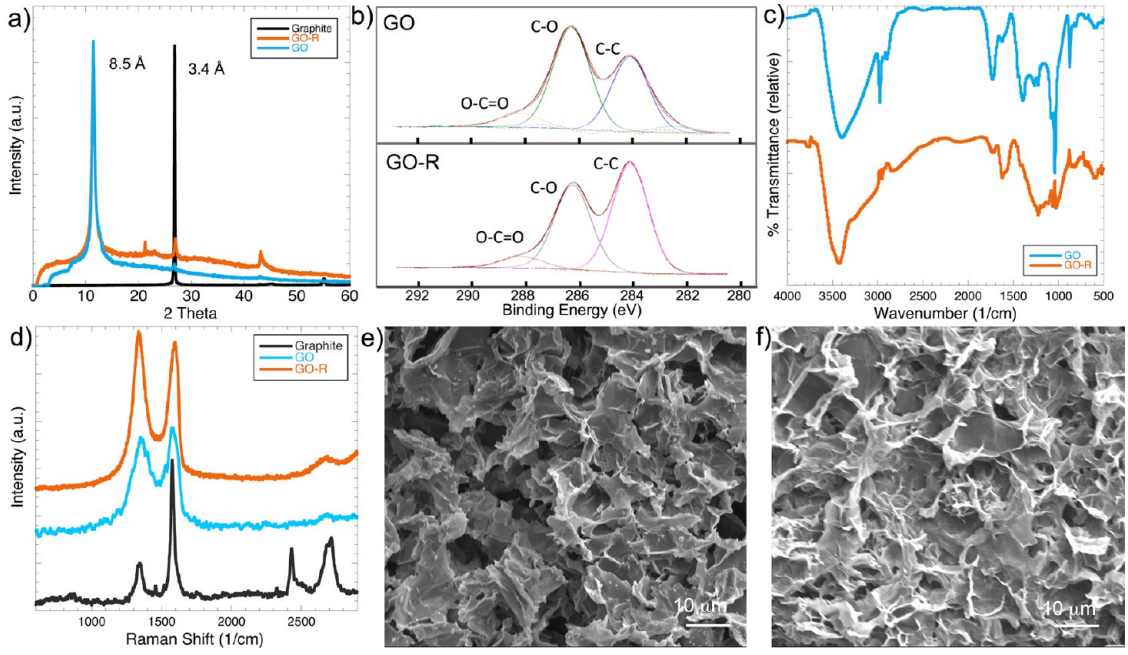

Figure 1. (a) X-ray diffractogram of pure graphite (black), GO-R (orange), and GO (blue). (b) X-ray photoelectron spectroscopy of the high-resolution carbon peak showing the increased presence of C−O bonded carbon in comparison to C−C bonded carbon in GO (top) *versus* GO-R (botton). (c) Fourier transform infrared spectra of the GO and GO-R showing the subtle differences in the proportion of oxygen functionalities arising from the oxidation state. (d) Raman spectra of graphite (black), GO-R (orange), and GO (blue) showing the polydispersity of layers and oxidation states in both GO-R and GO. G to D ratios were calculated to be 1.6:1, 0.78:1, and 0.77:1, respectively. SEM at 1000× of (e) GO and (f) GO-R cast from phosphate buffered saline solutions showing the exfoliated morphology of the material in the dried state.

system and thus cannot be assumed to be predictive of compatibility *in vivo*. Like other nanomaterials, the *in vivo* compatibility of GO remains poorly understood.[31] Of the studies that have evaluated the toxicity, compatibility, and clearance rates of GO *in vivo*, most have been performed in nonmammalian organisms; genotoxicity has been observed in *Caenorhabditis elegans*,[32] but findings in zebrafish suggest that GO is cleared rapidly and has no lasting effects.[33] In general, it is hypothesized that GO compatibility is governed by the type of functionalization[34] and its oxidation state.[24,33] However, only a few studies have endeavored to understand the compatibility of GO in mammals, and like previous work with CNTs, there is no consensus in the findings reported. Liu *et al.* reported that intravenous (IV) injection of GO in mice at 10−100 mg/mL induced mutagenesis,[35] while Liang *et al.* have reported that IV injection of GO showed no reproductive side effects even at high concentrations (25 mg/kg).[36] Others report no issues with safety when used in applications toward targeted delivery.[14,33,34] Efforts to understand the immune response to date have included characterization of the acute immune response following intraperitoneal (IP) injection.[37] Another study has attempted to understand the immune response induced by GO after IV injection,[38] reporting no systemic pathological changes in mice following administration of GO at low concentration. However, this report demonstrated significant inflammatory and immune responses when GO was administered at higher concentration (>10 mg/kg). To the best of our knowledge, no study has yet characterized the immune response when GO is administered by routes relevant for its use as a component in medical devices over a time course relevant for characterization of the foreign body reaction.

In this report, we evaluate the compatibility of GO in murine subcutaneous and intraperitoneal tissue sites, which are broadly relevant for the development of medical devices. In addition, we vary the degree of oxidation for GO to determine if a relationship exists between oxidative state and compatibility.

RESULTS AND DISCUSSION

GO used in these studies was synthesized by a modified Hummers method.[5] The amount of oxidizing reagents used in this synthesis was varied to produce distinct states of GO with different C to O ratios. Specifically, GO produced with the traditional stoichiometry gave a C to O ratio of 2.8:1 (GO, Supporting Information Figure S1a) and use of less potassium permanganate resulted in a form with a C to O ratio of 3.1:1 (GO-R, Supporting Information Figure S1b). No trace metal contamination, which could skew compatibility studies, was observed in either sample. Further characterization was carried out using X-ray photoelectron spectroscopy (XPS, Figure 1a), which showed that both GO and GO-R were fully exfoliated, indicated by the disappearance of the graphite *d*-spacing peak at 3.4 Å in the X-ray diffractogram and the appearance of

TABLE 1. Solution Properties of GO and GO-R

	C/O ratio	ζ (mV)	size, DI water (nm)	size, PBS (nm)	size, serum (nm)
GO	2.8:1	−29.0	1110	6380	13900
GO-R	3.1:1	−29.3	3420	3740	3280

a broad peak at 8.4 Å, characteristic of graphene oxide. The oxidation states are further confirmed in the high-resolution scan of the carbon peak in XPS (Figure 1b), where the relative intensity of the C−O component decreases compared to the C−C component for GO-R *versus* GO. Similarly in the Fourier transform infrared spectroscopy (FTIR) spectra (Figure 1c), the relative intensity of the C═O stretch characteristic of the peripheral lactones at 1725 cm^{-1} in relation to the C═O carboxylate peak at 1600 cm^{-1} decreases in GO-R *versus* GO. Raman spectroscopy was also used to characterize the samples (Figure 1d). As expected for a chemically oxidized graphenic material, GO and GO-R exist as a broad distribution of multilayer states, suggested by the shape and position of the G peak at 1600 cm^{-1} and the breadth of the G′ 2D peak at 2700 cm^{-1}.[39] G to D ratios were calculated to be 0.77:1 and 0.78:1 for GO and GO-R, respectively. Thermogravimentric analysis (TGA) shows the expected weight loss over the range from room temperature to 800 °C of around 40% (Supporting Information Figure S2).

We also characterized the solution properties of the material, as this is relevant for conditions experienced *in vivo*, and properties could differ greatly for characterization in the dry state compared to an aqueous environment. In solution, the particles of GO and GO-R were studied in deionized (DI) water, phosphate buffered saline (PBS), and serum to determine if salts and proteins in the body would have any effect on the aggregation state of the material. Incidentally, serum caused significant swelling of the GO particles, increasing the average particle size from 1110 to 16 200 nm. The size of the GO-R particles remained relatively constant at 3500 nm in the presence of PBS and serum (Table 1). Since dynamic light scattering (DLS) models may not accurately predict the size of a planar graphene particle, we verified these measurements using transmission electron microscopy (TEM) and observed a strong correlation for sizes measured in solution by DLS with those observed for dried films by TEM (Supporting Information Figure S3). Scanning electron microscopy (SEM) showed a consistent morphology for the material regardless of solution conditions or oxidation state (Figure 1e,f and Supporting Information Figure S4).

As mentioned, the compatibility of GO has largely been evaluated through an *in vitro* assessment of cytotoxicity. The preponderance of data in these studies has suggested that GO is not cytotoxic at moderate concentrations in solution. Therefore, we first sought to confirm these findings with the materials prepared here. A microvascular endothelial cell line (bEnd.3) and primary murine-derived mesenchymal stem cells were used as model cells relevant for applications in medical devices. Using a standard two-color live/dead cytotoxicity assay (Figure 2), it was determined that both GO and GO-R exhibited cytotoxicity at higher concentrations but were not cytotoxic at concentrations lower than 1 mg/mL in both cell types. There was a noted effect on cell proliferation at concentrations of 0.5 mg/mL or higher, as measured by an MTT assay (Supporting Information Figure S5). Both GO and GO-R exhibited similar cytotoxicity in these assays, and overall, these studies confirmed findings of minimal cytotoxicity at moderate concentrations reported in literature.

Simultaneously, to determine whether interactions with cells and biological components had any effect on the properties of graphene oxide, characterization was performed following exposure of GO and GO-R to endothelial cells. Qualitatively, the Raman spectra showed little change; however, the signal was lower, such that the G to D ratio could no longer be calculated with confidence and the G′ 2D peak was obscured (Supporting Information Figure S5). The increased noise in the Raman spectra could be a result of proteins adsorbed on the surface of GO, which implies that the graphene sheets may not directly interact with other cellular materials. To determine if the functional groups were altered following *in vitro* culture, FTIR spectra were collected for GO and GO-R (Supporting Information Figure S6). The spectrum of the isolated *in vitro* milieu was also taken as a control to ensure that any peaks observed in the GO or GO-R spectra were not simply due to the presence of substances from the cell culture. Significant changes were observed, especially in the nature of the carbonyl peaks. In both GO and GO-R, the C═O signal of the peripheral lactones at 1725 cm^{-1} disappeared completely, and the C═O of the carboxylate group at 1600 cm^{-1} increased in relative intensity.[6] This suggests that in the *in vitro* conditions, the peripheral lactones are opened to give carboxylate groups. An alternative explanation for this shift could be a change in pH.[40,41] However, the C═O peak is expected to become more pronounced at lower pH, suggesting that chemical interaction is a more likely explanation for the observed shifts. This offers an explanation to the reported observations that functional groups can modulate the compatibility of GO.[34]

The absence of toxicity *in vitro* does not necessarily dictate compatibility when a material is placed *in vivo*. The application of materials, such as GO, as medical devices would traditionally employ one of the following four routes of administration: (*i*) intravenous injection, (*ii*) subcutaneous implantation, (*iii*) intraperitoneal

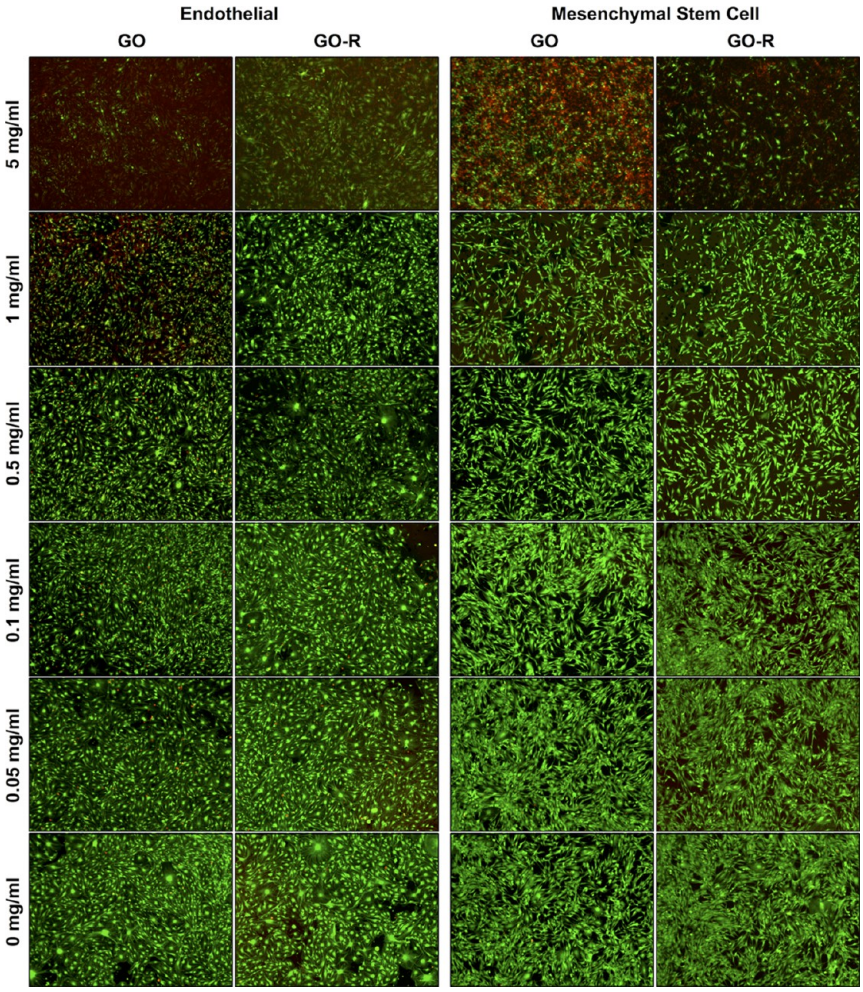

Figure 2. Representative images showing cytocompatibility of GO and GO-R in bEnd.3 microvascular endothelial cells (left) and mouse mesencyhmal stem cells (right) across a range of different graphene concentrations in media. Cells are stained with calcien AM (green, viable) and ethidium homodimer (red, not viable).

implantation, or (*iv*) direct administration to a specific tissue or organ. For intravenous administration, a general rule is that particle size must not exceed the diameter of a capillary (~4−5 μm).[42] However, nanomaterials that aggregate upon contact with blood may still have the potential to occlude pulmonary blood vessels. For the materials prepared here, intravenous administration of both GO-R and GO suspended in saline (dosed at either 2 or 20 mg/kg) resulted in lung occlusions within 1 min following administration, likely due to particle aggregation and/or swelling, like that observed *ex vivo* in the presence of serum. Hence, tissue compatibility of GO through this route of administration was not evaluated further.

Subcutaneous and peritoneal administration of a macroscopic implant is known to elicit a classic foreign body response.[43] Subcutaneous implants result in a cascade of cellular responses that begin with recruitment of neutrophils followed by monocytes.[43,44] These white blood cells secrete a variety of cytokines and chemokines, soluble immune-modulating signaling molecules, that result in the establishment of an inflammatory microenvironment at the interface of tissue and implant. In this microenvironment, monocytes differentiate into inflammatory macrophages, recruit fibroblasts, and form foreign body giant cells to encapsulate the implant.[43] Subcutaneous implantation through transcutaneous injection of GO or GO-R (20 mg/kg in 100 μL of saline) resulted in the formation of a coalesced mass of particles that resembled a macroscopic implant (Figure 3). As a result, we observe a classical macroscopic foreign body response against GO and GO-R when implanted subcutaneously. When comparing GO-R and GO upon excision of the implant and adjacent subcutaneous tissue, it was noted that the apparent size of the GO-R implant was considerably smaller in volume than that for GO, even though the implantation mass and volume were the same. There was also histological evidence of differences in these materials, as GO-R appeared to be more aggregated, while GO was more dispersed with the appearance of being hydrated. This is consistent with the solution properties of GO relative to GO-R in serum *ex vivo* (DLS and TEM), where considerable swelling

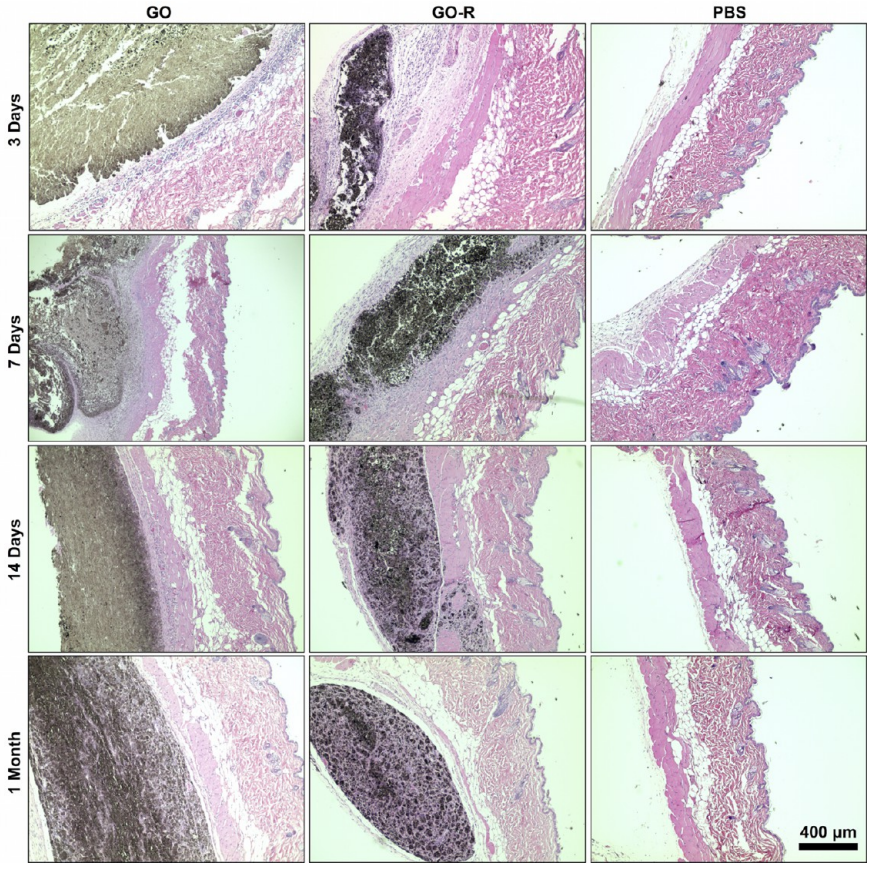

Figure 3. Subcutaneous tissue processed by standard histological methods and stained with hematoxylin and eosin (H&E). Representative images of the implant site shown for GO (left), GO-R (middle), and PBS (right) at 3 days, 7 days, 14 days, and 1 month.

was observed in a physiologic protein milieu. However, the tissue–material interface for both GO-R and GO had the appearance of a macroscopic device, and thus this interface was monitored over time in a manner consistent with routine biomedical device evaluation.

At 3 days following subcutaneous implantation, moderate monocyte infiltration was observed at the implant interface (Figure 3 and Supporting Information Figure S8). Infiltrating cells resulted in some observed damage and disorganization in the subcutaneous muscle tissue. When comparing GO-R to GO, there was a visible increase in monocyte presence at the interface for the GO-R samples. Substantial infiltration of monocytes within the GO-R macrostructure was also evident at this first time point, whereas GO remained primarily uninfiltrated. At both 7 and 14 days following implant, the margins of the GO macrostructure had begun to be infiltrated, and though some monocytes were still present, the majority of cells at this time were fibroblasts and macrophages. However, inflammatory cells had yet to penetrate throughout the material. Conversely, at both 7 and 14 days, GO-R was completely infiltrated with macrophages and fibroblasts. In both cases, the infiltrated material showed evidence of cell uptake and clearance. In both GO and GO-R, uptake was primarily by macrophages, with some evidence of multinucleated giant cells in each case. Additionally, clusters of GO-R exhibited some signs of mild fibrosis at 14 days postimplant, evident by diffuse staining of large aggregates using Mason's Trichrome staining (Supporting Information Figure S9). It is especially noteworthy that, by day 14, there were no signs of inflammation in the adjacent tissue, as subcutaneous muscle, adipose, and fascia layers appeared normal by histology with no increased presence of inflammatory cells. One month following implantation, GO was mostly infiltrated by macrophages, fibroblasts, and giant cells. GO-R remained completely infiltrated, and there was evidence of clearance and healing at the implant site. The implant and adjacent tissue showed signs of extensive angiogenesis, as the presence of blood vessels in and at the margins of the implant was dramatically increased. There was substantial *de novo* extracellular matrix production surrounding clusters of GO-R, but this matrix did not have fibrotic character, as evidenced in the Mason's Trichrome staining. GO, on the other hand, showed less matrix-specific staining, and clusters of GO still appeared more diffuse than GO-R.

In brief, both GO and GO-R demonstrated a canonical foreign body reaction following subcutaneous implantation. There was evidence of cell uptake by

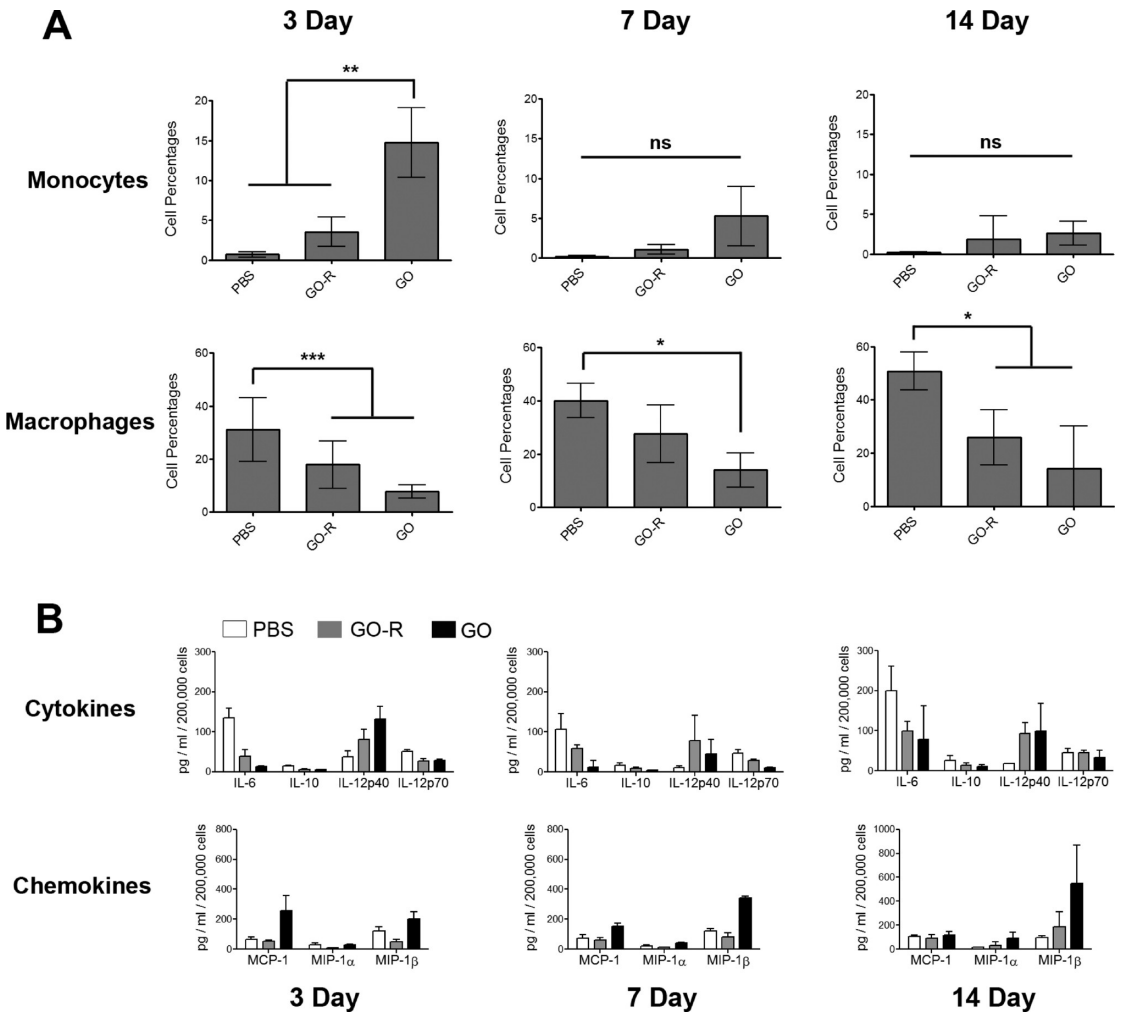

Figure 4. (A) Composition of cellular infiltrate in the peritoneal cavity following injection of graphene oxides. Monocytes and macrophage percentages measured 3 days, 7 days, and 14 days postinjection of graphene oxides or PBS; *$p < 0.05$, **$p < 0.01$, and ***$p < 0.001$. Data are based on $n \geq 3$ and are represented as mean $\pm$ SD. (B) Cytokines and chemokines secreted by cells of the peritoneal cavity. Amounts secreted by cells upon overnight culture and measured using a 32-plex luminex assay, of which 7 cytokines/chemokines are listed here. Significant differences in levels of IL-12p40, MCP-1, and MIP-1β were observed. Statistical analysis of secreted protein levels is provided in Supporting Information Table S1. Data are based on $n = 3$ and are represented as mean + SD.

macrophages and giant cells in both cases, as well as indications of material clearance from site of injection. The dependence of the observed response on oxidation state may possibly be attributable to the differences in hydration of the macroscopic mass of GO particles; specifically, the aggregated nature of the GO-R particles facilitated more infiltration and interpenetration of immune cells, as well as increased uptake by macrophages. Conversely, the more hydrated macroscopic implant of GO particles was slower to be infiltrated and phagocytosed. Additionally, the nature of the surface functional groups could play a role, as suggested by the *ex vivo* data discussed above.

GO and GO-R were injected IP at the same dose as was administered subcutaneously (20 mg/kg in 100 μL of saline). At serial time points following administration, a peritoneal lavage was performed, and the presence of inflammatory cells was identified and quantified using flow cytometry (Supporting Information Figure S10) and compared to a control injection of PBS. Macrophage levels were significantly reduced in comparison to the PBS control until 2 weeks following administration. In contrast, Ly6C$^+$ monocyte levels were significantly elevated in the peritoneal exudate 3 days following GO administration when compared to both GO-R and control, which continued until 2 weeks following administration (Figure 4A). The increase in monocytes following GO injection correlated with an increased functional capacity of peritoneal exudate cells to establish an inflammatory microenvironment, as measured by the increased secretion of inflammatory cytokines and chemokines (Figure 4B). *Ex vivo* cytokine and chemokine secretion levels from peritoneal exudate cells, determined using an array method to quantify 32 different immune-modulating cytokines and chemokines (Supporting Information Figure S11),

demonstrated significant differences in the secretion of cytokines and chemokines commonly associated with inflammation.[45,46] Specifically, cells retrieved from GO-injected mice at both 3 and 7 days following implantation secreted significantly greater amounts of the inflammatory cytokine subunit IL-12p40 (a component of both IL-12 and IL-23) and inflammatory chemokines, monocyte chemotactic protein-1 (MCP-1) and macrophage inflammatory protein-1β (MIP-1β), compared to GO-R-injected mice (Figure 4B and Supporting Information Table S1). However, there were no significant changes in the secretion of IL-12p70 or MIP-1α or in the anti-inflammatory cytokine IL-10. Interestingly, significantly lower levels of the cytokine IL-6 was secreted by cells from both GO- and GO-R-injected mice when compared to control mice. IL-6 is a pleiotropic cytokine that has been shown to have protective effects and is known to be secreted by various tissues in the body in homeostasis.[47,48] Additionally, it is capable of suppressing acute inflammatory responses by reducing neutrophil recruitment and altering secretion of other inflammatory cytokines.[48−50] It is possible that the IL-6 levels observed in mice from our control group are normal in the peritoneal cavity and are lowered during acute inflammation resulting from the injection of GO or GO-R. Finally, the clearance rate of material from the IP space was dependent on oxidation level, with GO-R visibly being cleared faster than GO upon gross inspection of the peritoneal exudate (Supporting Information Figure S12). Examination of histological sections of the liver and spleen using traditional microscopic techniques showed no gross morphological changes in these organs, suggestive of systemic compatibility and a lack of acute toxicity (Supporting Information Figure S13).

In summary, intraperitoneal administration of GO and GO-R resulted in a characteristic inflammatory response with recruitment of monocytes and increases in inflammatory cytokine and chemokine secretion when compared to PBS administration. The reduced inflammatory response in response to GO-R when compared to GO administration could possibly be a result of the differences in the kinetics of clearance rates from the site of injection, which may be related to their surface hydrophilicity and functional groups, as well as differences in aqueous dispersibility. GO-R, with reduced surface oxidation, could potentially be taken up by infiltrating monocytes[51] soon after administration. Similar to the effects observed following subcutaneous implantation, the clearance rate of GO is slower, resulting in increased accumulation of inflammatory monocytes in the peritoneal exudates.

CONCLUSIONS

We have evaluated the compatibility for GO of two different oxidation levels following implantation in subcutaneous and peritoneal tissue sites, which are of broad relevance for application to medical devices. Overall, GO was demonstrated to be moderately compatible in both tissue sites, eliciting an inflammatory response consistent with a typical foreign body reaction. A reduction in the degree of GO oxidation resulted in more rapid immune cell infiltration, uptake, and clearance from the injection site following subcutaneous implantation. Uptake occurred on the order of weeks and resulted from infiltrating monocytes, macrophages, and multinucleated giant cells. Though the implant had dense infiltration of immune cells, the adjacent tissue showed no signs of inflammation or injury as a result of GO implantation. Following IP administration, GO with higher oxidation resulted in increased accumulation of monocytes and an enhanced pro-inflammatory environment. Meanwhile, GO-R was more rapidly cleared from the IP space and demonstrated less chronic inflammation.

Future work should focus on ascertaining and controlling the clearance mechanisms to fully exploit the potential of this material. Additional work toward covalent modification or noncovalent coating of graphene oxide could also promote a reduction in inflammatory response and improve its compatibility as a component of medical devices. Nevertheless, a foreign body reaction can be expected from any medical device, and the severity of that observed here is thought to be acceptable. It is hoped that the information provided through these studies, showing a transient cell-mediated immune response and cell uptake, can inform the use of graphene oxide as a material for scaffolds, controlled release, and other medical applications.

MATERIALS AND METHODS

Preparation and Characterization of Graphene Oxide. *Synthesis of GO.* In a typical experiment, 5 g of graphite (Alfa Aesar, 325 mesh, 99.9995% metal basis) was added to 125 mL of concentrated sulfuric acid (H_2SO_4, 95%) in a 1 L open heavy-walled reaction vessel over ice behind a blast shield. These reagents were allowed to stir vigorously for 10 min, at which point 10 g of fresh potassium permanganate ($KMnO_4$) was slowly added over the next 20 min. After the addition was complete, the ice bath was removed and the reaction was allowed to warm to room temperature over 30 min. At this time, a water bath was added and the reaction was gently heated at 35 °C for an additional 2 h. After 2 h, the reaction was quenched *via* the slow addition of 700 mL of DI water, followed by 10 mL of hydrogen peroxide solution (H_2O_2, 30% in water), followed by 225 mL of DI water. The quenched dispersion was allowed to stir overnight. On the following morning, the solids were collected *via* centrifugation and the graphene oxide was purified *via* dialysis against DI water for 1 week. The solids were lyophilized to typically yield of about 10 g of GO (73.7% C, 26.3% O), which was characterized by FTIR, TGA, Raman, SEM, TEM, XPS, DLS, and XRD.

Synthesis of GO-R. The same procedure used to synthesize GO was applied using 5 g of graphite and 7.5 g of potassium permanganate. Lyophilization typically yielded about 8 g of GO-R (75.6% C, 24.4% O), which was again characterized by FTIR, TGA, Raman, SEM, TEM, XPS, DLS, and XRD.

Material Characterization. FTIR spectra were determined using a Nexus model 670 spectrophotometer using the Omnic software package. TGA was performed using a TA Instruments Q50 under nitrogen at a scan rate of 15 °C/min from 50 to 800 °C. X-ray diffraction was measured using Cu Kα radiation on an Inel CPS 120 position-sensitive detector with a XRG 3000 generator using a 20 min collection time. ζ-Potentials and particle sizes were measured in water using a Brookhaven Instruments Corporation phase analysis light scattering (PALS) ζ-potential analyzer. All values are an average of ten 10 s scans. XPS spectra were recorded and processed using a Physical Electronics Versaprobe II X-ray photoelectron spectrometer. Raman spectra were recorded on a Horiba Lab Ram equipped with a 533 nm YAG laser using LabSpec 5 processing software. SEM was performed on gold-coated samples using a JEOL 6010LA microscope with a tungsten source and an SEI detector. TEM was performed using a FEI Tecnai G2 Spirit TWIN microscope. Samples were prepared on lacey carbon or copper grids.

***In Vitro* Assessment of Cytotoxicity.** bEnd.3 and RAW 264.7 were obtained from American Type Culture Collection (ATCC, Manassas, VA, USA) and cultured in Dulbecco's modified Eagle's medium (DMEM) (low glucose containing L-glutamine and sodium pyruvate, Life Technologies, Grand Island, NY, USA) containing 10% fetal bovine serum and 1% antibiotics. Mouse mesenchymal stem cells were obtained from Life Technologies (Grand Island, NY, USA) and cultured according to the manufacturer's instructions. To assess cytocompatibility, 100 000 cells were plated onto a 48-well cell culture plate, and 48 h later, 500 μg of graphene oxide in 100 μL of PBS was added. Following overnight culture in the presence of GO, cell viability was assessed using a two-color live–dead cytotoxicity kit (Life Technologies) using calcien AM (live, green) and ethidium homodimer (dead, red) to establish cell viability. Following staining, cells were imaged on an EVOS fluorescence microscope. MTT cell proliferation assay was purchased from Life Technologies (Grand Island, NY, USA) and performed according to manufacturer's instructions.

***In Vivo* Assessment of Compatibility.** Wild-type 8–10 week old male C57BL/6J mice (Jackson Laboratories) were used in all studies. Animal studies were performed in accordance with protocols approved by MIT's committee for animal care and followed all local, state, and federal regulations. Mice were housed in MIT's division of comparative medicine facilities and provided with food and water *ad libitum*.

Graphene oxide solutions in PBS were prepared under sterile conditions. A 20 mg/kg dose (which corresponds to approximately 0.5 mg of GO per mouse) or 2 mg/kg dose (which corresponds to approximately 0.05 mg of GO per mouse) of GO was administered per mouse in 100 μL of PBS, using a 27 gauge, 0.5 cm^3 insulin syringe. For subcutaneous injections, the back of the mouse was shaved and cleaned using 70% ethanol prior to injections. To limit variability between mice, each mouse received a subcutaneous injection of PBS, GO, and GO-R at three different sites within the same animal. For intraperitoneal injections, each mouse was randomly assigned to receive an injection of one of PBS, GO, or GO-R. At desired time points, mice were euthanized and the subcutaneous tissue in and around the area of PBS, GO, and GO-R administration was dissected. Tissue was immediately transferred to 10% formalin fixative prior to sectioning and staining at the Histology Core Facility at MIT. Hematoxylin and eosin or Masson's Trichrome staining was performed on slides containing sectioned tissue, and the stained slides were analyzed using an EVOS color microscope (Life Technologies). For peritoneal administration, at desired time points, mice were euthanized and the peritoneum was infused with 5 mL of cold PBS. Injected PBS along with peritoneal exudate (containing immune cells) was retrieved, passed through a 70 μm filter, and stored on ice prior to further analysis. Cells from peritoneal exudate were counted using an automated Countess (Life Technologies) cell counter. Counted cells were cultured in a 96-well plate overnight in DMEM media (as above). Supernatants from these cultures were collected frozen prior to analysis using a 32-plex Bioplex cytokine assay (Bio-Rad, Hercules, CA, USA). Another part of the cells was stained with the following antibodies against cell-surface proteins: CD11b (clone M1/70), Ly6G (1A8), Ly6C (HK1.4), CD19 (6D5), TCRβ (H57-597), F4/80 (BM8), and CD11c (N418) (all from Biolegend, San Diego, CA, USA), in the presence of Fc Block for 20 min at 4 °C. Flow cytometry data were collected using a BD LSR-II or BD LSR-Fortessa, and the data were analyzed using Flow FlowJo (Tree Star Inc., Ashland, OR, USA).

Conflict of Interest: The authors declare no competing financial interest.

Acknowledgment. This work was supported by the National Institutes of Health (NIDCR) Research Project Grant Program (R01-DE016516-06) and the National Institutes of Health Centers for Cancer Nanotechnology Excellence (1U54CA151884-01). S.A.S. acknowledges support from the National Institutes of Health (NIBIB) through a Ruth L. Kirschstein National Research Service Award (F32EB018155). S.J. is in receipt of the Mazumdar-Shaw International Oncology Fellowship. M.J.W. acknowledges support from the National Institutes of Health (NIDDK) through a Ruth L. Kirschstein National Research Service Award (F32DK101335). The authors would like to thank Zoe Wright for her assistance in artistic rendering in the manuscript.

Supporting Information Available: Elemental analysis of graphene oxide *via* low-resolution XPS, TGA, TEM, and SEM of graphene oxides, MTT assay, characterization of graphene oxides using Raman and FTIR, H&E, and Masson's Trichrome stains of subcutaneous tissue implanted with graphene oxide, flow cytometry gating strategy, cytokine and chemokines secreted by IP cells, images of IP exudate, liver and spleen histology, table of *p* values for data presented in Figure 4B. This material is available free of charge *via* the Internet at http://pubs.acs.org.

REFERENCES AND NOTES

1. Geim, A. K. Graphene: Status and Prospects. *Science* **2009**, *324*, 1530–1534.
2. Kim, H.; Abdala, A. A.; Macosko, C. W. Graphene/Polymer Nanocomposites. *Macromolecules* **2010**, *43*, 6515–6530.
3. Di, C.-A.; Wei, D.; Yu, G.; Liu, Y.; Guo, Y.; Zhu, D. Patterned Graphene as Source/Drain Electrodes for Bottom-Contact Organic Field-Effect Transistors. *Adv. Mater.* **2008**, *20*, 3289–3293.
4. Ang, P. K.; Li, A.; Jaiswal, M.; Wang, Y.; Hou, H. W.; Thong, J. T. L.; Lim, C. T.; Loh, K. P. Flow Sensing of Single Cell by Graphene Transistor in a Microfluidic Channel. *Nano Lett.* **2011**, *11*, 5240–5246.
5. Hummers, W. S.; Offeman, R. E. Preparation of Graphitic Oxide. *J. Am. Chem. Soc.* **1958**, *80*, 1339–1339.
6. Dreyer, D. R.; Park, S.; Bielawski, C. W.; Ruoff, R. S. The Chemistry of Graphene Oxide. *Chem. Soc. Rev.* **2010**, *39*, 228–240.
7. Shin, H.-J.; Kim, K. K.; Benayad, A.; Yoon, S.-M.; Park, H. K.; Jung, I.-S.; Jin, M. H.; Jeong, H.-K.; Kim, J. M.; Choi, J.-Y.; Lee, Y. H. Efficient Reduction of Graphite Oxide by Sodium Borohydride and Its Effect on Electrical Conductance. *Adv. Funct. Mater.* **2009**, *19*, 1987–1992.
8. Suk, J. W.; Piner, R. D.; An, J.; Ruoff, R. S. Mechanical Properties of Monolayer Graphene Oxide. *ACS Nano* **2010**, *4*, 6557–6564.
9. Collins, W. R.; Schmois, E.; Swager, T. M. Graphene Oxide as an Electrophile for Carbon Nucleophiles. *Chem. Commun.* **2011**, *47*, 8790–8792.
10. Sydlik, S. A.; Swager, T. M. Functional Graphenic Materials *via* a Johnson–Claisen Rearrangement. *Adv. Funct. Mater.* **2013**, *23*, 1873–1882.
11. Chapman, R. G.; Ostuni, E.; Takayama, S.; Holmlin, R. E.; Yan, L.; Whitesides, G. M. Surveying for Surfaces That Resist the Adsorption of Proteins. *J. Am. Chem. Soc.* **2000**, *122*, 8303–8304.

12. Fan, H.; Wang, L.; Zhao, K.; Li, N.; Shi, Z.; Ge, Z.; Jin, Z. Fabrication, Mechanical Properties, and Biocompatibility of Graphene-Reinforced Chitosan Composites. *Biomacromolecules* **2010**, *11*, 2345–2351.
13. Zhang, W.; Guo, Z.; Huang, D.; Liu, Z.; Guo, X.; Zhong, H. Synergistic Effect of Chemo-photothermal Therapy Using PEGylated Graphene Oxide. *Biomaterials* **2011**, *32*, 8555–8561.
14. Yang, K.; Zhang, S.; Zhang, G.; Sun, X.; Lee, S.-T.; Liu, Z. Graphene in Mice: Ultrahigh *In Vivo* Tumor Uptake and Efficient Photothermal Therapy. *Nano Lett.* **2010**, *10*, 3318–3323.
15. Yang, K.; Wan, J.; Zhang, S.; Tian, B.; Zhang, Y.; Liu, Z. The Influence of Surface Chemistry and Size of Nanoscale Graphene Oxide on Photothermal Therapy of Cancer Using Ultra-low Laser Power. *Biomaterials* **2012**, *33*, 2206–2214.
16. Ma, X.; Tao, H.; Yang, K.; Feng, L.; Cheng, L.; Shi, X.; Li, Y.; Guo, L.; Liu, Z. A Functionalized Graphene Oxide-Iron Oxide Nanocomposite for Magnetically Targeted Drug Delivery, Photothermal Therapy, and Magnetic Resonance Imaging. *Nano Res.* **2012**, *5*, 199–212.
17. Sun, X.; Liu, Z.; Welsher, K.; Robinson, J.; Goodwin, A.; Zaric, S.; Dai, H. Nano-graphene Oxide for Cellular Imaging and Drug Delivery. *Nano Res.* **2008**, *1*, 203–212.
18. Zhang, L.; Xia, J.; Zhao, Q.; Liu, L.; Zhang, Z. Functional Graphene Oxide as a Nanocarrier for Controlled Loading and Targeted Delivery of Mixed Anticancer Drugs. *Small* **2010**, *6*, 537–544.
19. Chen, G. Y.; Pang, D. W. P.; Hwang, S. M.; Tuan, H. Y.; Hu, Y. C. A Graphene-Based Platform for Induced Pluripotent Stem Cell Culture and Differentiation. *Biomaterials* **2012**, *33*, 418–427.
20. Nayak, T. R.; Andersen, H.; Makam, V. S.; Khaw, C.; Bae, S.; Xu, X.; Ee, P.-L. R.; Ahn, J.-H.; Hong, B. H.; Pastorin, G.; Özyilmaz, B. Graphene for Controlled and Accelerated Osteogenic Differentiation of Human Mesenchymal Stem Cells. *ACS Nano* **2011**, *5*, 4670–4678.
21. Toyokuni, S. Genotoxicity and Carcinogenicity Risk of Carbon Nanotubes. *Adv. Drug Delivery Rev.* **2013**, *65*, 2098–2110.
22. Machado, N. M.; Lopes, J. C.; Saturnino, R. S.; Fagan, E. B.; Nepomuceno, J. C. Lack of Mutagenic Effect by Multi-walled Functionalized Carbon Nanotubes in the Somatic Cells of *Drosophila melanogaster*. *Food Chem. Toxicol.* **2013**, *62*, 355–360.
23. Dimiev, A. M.; Alemany, L. B.; Tour, J. M. Graphene Oxide. Origin of Acidity, Its Instability in Water, and a New Dynamic Structural Model. *ACS Nano* **2012**, *7*, 576–588.
24. Duch, M. C.; Budinger, G. R. S.; Liang, Y. T.; Soberanes, S.; Urich, D.; Chiarella, S. E.; Campochiaro, L. A.; Gonzalez, A.; Chandel, N. S.; Hersam, M. C.; Mutlu, G. M. Minimizing Oxidation and Stable Nanoscale Dispersion Improves the Biocompatibility of Graphene in the Lung. *Nano Lett.* **2011**, *11*, 5201–5207.
25. Lee, W. C.; Lim, C. H. Y. X.; Shi, H.; Tang, L. A. L.; Wang, Y.; Lim, C. T.; Loh, K. P. Origin of Enhanced Stem Cell Growth and Differentiation on Graphene and Graphene Oxide. *ACS Nano* **2011**, *5*, 7334–7341.
26. Menaa, F.; Abdelghani, A.; Menaa, B. Graphene Nanomaterials as Biocompatible and Conductive Scaffolds for Stem Cells: Impact for Tissue Engineering and Regenerative Medicine. *J. Tissue Eng. Regen. Med.* **2014**, 10.1002/term.1910.
27. Sanchez, V. C.; Jachak, A.; Hurt, R. H.; Kane, A. B. Biological Interactions of Graphene-Family Nanomaterials: An Interdisciplinary Review. *Chem. Res. Toxicol.* **2011**, *25*, 15–34.
28. Seabra, A. B.; Paula, A. J.; de Lima, R.; Alves, O. L.; Durán, N. Nanotoxicity of Graphene and Graphene Oxide. *Chem. Res. Toxicol.* **2014**, *27*, 159–168.
29. Chen, G. Y.; Yang, H. J.; Lu, C. H.; Chao, Y. C.; Hwang, S. M.; Chen, C. L.; Lo, K. W.; Sung, L. Y.; Luo, W. Y.; Tuan, H. Y.; Hu, Y. C. Simultaneous Induction of Autophagy and Toll-like Receptor Signaling Pathways by Graphene Oxide. *Biomaterials* **2012**, *33*, 6559–6569.
30. Qu, G.; Liu, S.; Zhang, S.; Wang, L.; Wang, X.; Sun, B.; Yin, N.; Gao, X.; Xia, T.; Chen, J. J.; Jiang, G. B. Graphene Oxide induces Toll-like Receptor 4 (TLR4)-Dependent Necrosis in Macrophages. *ACS Nano* **2013**, *7*, 5732–5745.
31. Kostarelos, K.; Novoselov, K. S. Materials Science. Exploring the Interface of Graphene and Biology. *Science* **2014**, *344*, 261–263.
32. Wu, Q.; Zhao, Y.; Li, Y.; Wang, D. Molecular Signals Regulating Translocation and Toxicity of Graphene Oxide in the Nematode *Caenorhabditis elegans*. *Nanoscale* **2014**, *6*, 11204–11212.
33. Liu, C. W.; Xiong, F.; Jia, H. Z.; Wang, X. L.; Cheng, H.; Sun, Y. H.; Zhang, X. Z.; Zhuo, R. X.; Feng, J. Graphene-Based Anticancer Nanosystem and Its Biosafety Evaluation Using a Zebrafish Model. *Biomacromolecules* **2013**, *14*, 358–366.
34. Liu, J.; Cui, L.; Losic, D. Graphene and Graphene Oxide as New Nanocarriers for Drug Delivery Applications. *Acta Biomater.* **2013**, *9*, 9243–9257.
35. Liu, Y.; Luo, Y.; Wu, J.; Wang, Y.; Yang, X.; Yang, R.; Wang, B.; Yang, J.; Zhang, N. Graphene Oxide Can Induce *In Vitro* and *In Vivo* Mutagenesis. *Sci. Rep.* **2013**, *3*, 3469.
36. Liang, S.; Xu, S.; Zhang, D.; He, J.; Chu, M. Reproductive Toxicity of Nanoscale Graphene Oxide in Male Mice. *Nanotoxicology* **2015**, *9*, 92–105.
37. Ali-Boucetta, H.; Bitounis, D.; Raveendran-Nair, R.; Servant, A.; Van den Bossche, J.; Kostarelos, K. Purified Graphene Oxide Dispersion Lack *In Vitro* Cytotoxicity and *In Vivo* Pathogenicity. *Adv. Healthcare Mater.* **2013**, *2*, 433–441.
38. Zhang, X.; Yin, J.; Peng, C.; Hu, W.; Zhu, Z.; Li, W.; Fan, C.; Huang, Q. Distribution and Biocompatibility Studies of Graphene Oxide in Mice after Intravenous Administration. *Carbon* **2011**, *49*, 986–995.
39. Malard, L.; Pimenta, M.; Dresselhaus, G.; Dresselhaus, M. Raman Spectroscopy in Graphene. *Phys. Rep.* **2009**, *473*, 51–87.
40. Niemeyer, J.; Chen, Y.; Bollag, J.-M. Characterization of Humic Acids, Composts, and Peat by Diffuse Reflectance Fourier-Transform Infrared Spectroscopy. *Soil Sci. Soc. Am. J.* **1992**, *56*, 135–140.
41. Cabaniss, S. E.; McVey, I. F. Aqueous Infrared Carboxylate Absorbances: Aliphatic Monocarboxylates. *Spectrochim. Acta. A* **1995**, *51*, 2385–2395.
42. Ross, J. J. *Best and Taylor's Physiological Basis of Medical Practice*, 12th ed.; Williams & Wilkins: Baltimore, MD, 1991.
43. Anderson, J. M.; Rodriguez, A.; Chang, D. T. Foreign Body Reaction to Biomaterials. *Semin. Immunol.* **2008**, *20*, 86–100.
44. Luttikhuizen, D. T.; Harmsen, M. C.; Van Luyn, M. J. Cellular and Molecular Dynamics in the Foreign Body Reaction. *Tissue Eng.* **2006**, *12*, 1955–1970.
45. Mackay, C. R. Chemokines: Immunology's High Impact Factors. *Nat. Immunol.* **2001**, *2*, 95–101.
46. Vignali, D. A.; Kuchroo, V. K. IL-12 Family Cytokines: Immunological Playmakers. *Nat. Immunol.* **2012**, *13*, 722–728.
47. Jones, S. A.; Horiuchi, S.; Topley, N.; Yamamoto, N.; Fuller, G. M. The Soluble Interleukin 6 Receptor: Mechanisms of Production and Implications in Disease. *FASEB J.* **2001**, *15*, 43–58.
48. Hurst, S. M.; Wilkinson, T. S.; McLoughlin, R. M.; Jones, S.; Horiuchi, S.; Yamamoto, N.; Rose-John, S.; Fuller, G. M.; Topley, N.; Jones, S. A. IL-6 and Its Soluble Receptor Orchestrate a Temporal Switch in the Pattern of Leukocyte Recruitment Seen during Acute Inflammation. *Immunity* **2001**, *14*, 705–714.
49. Xing, Z.; Gauldie, J.; Cox, G.; Baumann, H.; Jordana, M.; Lei, X. F.; Achong, M. K. IL-6 Is an Antiinflammatory Cytokine Required for Controlling Local or Systemic Acute Inflammatory Responses. *J. Clin. Invest.* **1998**, *101*, 311–320.
50. Schindler, R.; Mancilla, J.; Endres, S.; Ghorbani, R.; Clark, S. C.; Dinarello, C. A. Correlations and Interactions in the Production of Interleukin-6 (IL-6), IL-1, and Tumor Necrosis Factor (TNF) in Human Blood Mononuclear Cells: IL-6 Suppresses IL-1 and TNF. *Blood* **1990**, *75*, 40–47.
51. Smith, B. R.; Ghosn, E. E.; Rallapalli, H.; Prescher, J. A.; Larson, T.; Herzenberg, L. A.; Gambhir, S. S. Selective Uptake of Single-Walled Carbon Nanotubes by Circulating Monocytes for Enhanced Tumour Delivery. *Nat. Nanotechnol.* **2014**, *9*, 481–7.